35th Annual International Conference of the IEEE EMBS
Osaka, Japan, 3 - 7 July, 2013

Optimizing bipolar radiofrequency ablation treatment by means of pulsed currents

Frederik Soetaert, Guillaume Crevecoeur and Luc Dupré

***Abstract*— Given the high mortality rate, liver cancer is considered to be a difficult cancer to treat. Consequently, alternative strategies are being developed such as radiofrequency ablation (RFA). RFA applies radiofrequent currents leading to local heating of the tumoral tissue. Accurate numerical modeling contributes to a better knowledge of the physical phenomena and allows optimizations. In this work, the bipolar radiofrequency ablation technique is explored followed by an optimization by means of pulsed currents. Numerical results clearly show the larger ablation zones due to the pulsed currents. Hence, pulsed bipolar RFA increases the efficacy and has the potential to be incorporated in clinical practice.**

I. INTRODUCTION

Conventional therapies for cancer are mostly a combination of surgery, chemo- and radiotherapy. These cancer therapies are not always an effective treatment, in particular when treating liver cancer, one of the most occurring forms of cancer. Primary liver tumors, so-called hepatocellular carcinoma (HCC), occur approximately in 749000 cases per year [1]. Unfortunately, the five year survival rate for HCC is only 12% [2]. Therefore, alternative strategies are explored so to increase this survival rate.

Thermotherapy is such a recently developed technique that consists in applying heat in the tumoral tissue. The tissue can be heated by means of cryoablation, microwave ablation or radiofrequency ablation [3]. Radiofrequency ablation (RFA) heats the tissue through the use of one or multiple electrodes injecting radiofrequent currents. Contrary to previous studies, we focus on bipolar RFA devices. In a bipolar configuration, we use two electrodes that are driven by a current source (Fig. 1). This technique is not yet well understood and engineering research is needed so to increase the efficacy of this method.

This study presents numerical methods for a bipolar RFA configuration. The numerical model consists of two coupled subproblems: the electrical and thermal subproblem. First, a Poisson differential equation is solved in order to simulate the electrical fields originating from the injected currents. Secondly, the thermal phenomena are characterized by the so-called Pennes bioheat equation for given heat sources and heat sinks. Both numerical methods are finite difference based.

Furthermore, we propose the use of pulsed currents to improve the efficacy of the bipolar configuration. Our propositions are supported by the numerical results.

Frederik Soetaert, Guillaume Crevecoeur and Luc Dupré are with the Department of Electrical Energy, Systems and Automation, Ghent University, Sint-Pietersnieuwstraat 41, B-9000 Ghent, Belgium. frederik.soetaert at ugent.be

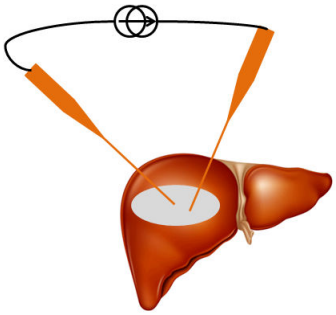

Fig. 1. Schematic representation of a bipolar configuration for RFA.

II. METHODS

A. Numerical model

The numerical model of RFA consists of two subproblems describing the electrical and the thermal physical phenomena. In addition, these two subproblems are strongly coupled to each other.

The electrical phenomena in RFA are modeled by expressing the continuity equation resulting in a Poisson equation:

$$\nabla \cdot \left[\sigma\left(\vec{r}\right)\nabla\phi\left(\vec{r},t\right)\right] = I_0\,\delta\left(\vec{r}-\vec{r}_1\right) - I_0\,\delta\left(\vec{r}-\vec{r}_2\right) \quad (1)$$

Here ϕ represents the electrical potential (V) and σ is the electrical conductivity $\left(\frac{\mathrm{S}}{\mathrm{m}}\right)$, as a function of space $(\vec{r})$ and time (t). I_0 is the volumetric current density $\left(\frac{\mathrm{A}}{\mathrm{m}^3}\right)$ caused by the electrodes at places $\vec{r}_1$ and $\vec{r}_2$. Additionally, we use a Dirichlet type boundary condition for (1). The resulting electrical field $\vec{E} = -\nabla\phi\left(\frac{\mathrm{V}}{\mathrm{m}}\right)$ generates Joule heating $\left(\frac{\mathrm{W}}{\mathrm{m}^3}\right)$:

$$q_E = \sigma\left(\vec{r},T\left(\vec{r},t\right)\right)\left|\vec{E}\left(\vec{r},t\right)\right|^2 \quad (2)$$

The thermal subproblem consists in calculating the temperature distribution during an RFA treatment. RFA introduces q_E as an additional heat source next to the biological heat transfer model of Pennes [4], [5]:

$$\rho\left(\vec{r}\right)c\left(\vec{r}\right)\frac{\partial T\left(\vec{r},t\right)}{\partial t} = \nabla\cdot\left[k\left(\vec{r},T\left(\vec{r},t\right)\right)\nabla T\left(\vec{r},t\right)\right]$$
$$-\alpha\left(\vec{r},t\right)\omega\rho_b c_b\left(T\left(\vec{r},t\right)-T_c\right) + q_E \quad (3)$$

The left-hand side of this partial differential equation consists of the temperature T (K), the mass density of the tissue ρ $\left(\frac{\mathrm{kg}}{\mathrm{m}^3}\right)$ and the specific heat capacity of the tissue c $\left(\frac{\mathrm{J}}{\mathrm{kg}\cdot\mathrm{K}}\right)$. The right-hand side contains the different heat sources and sinks. The first term describes the traditional heat conduction with the thermal conductivity k $\left(\frac{\mathrm{W}}{\mathrm{m}\cdot\mathrm{K}}\right)$. The second term is a measure for the effect of blood perfusion. The blood and

978-1-4577-0216-7/13/$26.00 ©2013 IEEE

TABLE I

BLOOD PROPERTIES [6].

Symbol (unit)	Value
$\omega \ \left(\mathrm{s}^{-1}\right)$	0.0064
$c_b \ \left(\mathrm{J\ kg^{-1}K^{-1}}\right)$	4180
$\rho_b \ \left(\mathrm{kg\ m^{-3}}\right)$	1000

TABLE II

MATERIAL PROPERTIES OF HEALTHY AND TUMORAL LIVER TISSUE [5].

Symbol (unit)	Healthy tissue	Tumoral tissue
$\rho \ \left(\mathrm{kg\ m^{-3}}\right)$	1016	1016
$c \ \left(\mathrm{J\ kg^{-1}\ K^{-1}}\right)$	3500	3500
$\sigma_0 \ \left(\mathrm{S\ m^{-1}}\right)$	0.36	0.45
$\sigma_1 \ \left(\mathrm{K^{-1}}\right)$	0.015	0.015
$k_0 \ \left(\mathrm{W\ m^{-1}\ K^{-1}}\right)$	0.53	0.53
$k_1 \ \left(\mathrm{W\ m^{-1}\ K^{-2}}\right)$	0.00116	0.00116

tissue material properties in this study are summarized in table I and II.

In order to obtain a correct interpretation for thermotherapy, we employed an Arrhenius model for the thermal damage caused by RFA [7]:

$$\alpha\left(\vec{r},t\right)=\exp\left[-\int_0^t Ae^{-\frac{\Delta E_a}{R\cdot T\left(\vec{r},t'\right)}}\,\mathrm{d}t'\right] \tag{4}$$

with the gas constant R, frequency factor A $\left(2.984\cdot10^{80}\,\mathrm{s}^{-1}\right)$ and ΔE_a $\left(5.064\cdot10^{5}\,\mathrm{J\ mol}^{-1}\right)$ as the activation energy barrier [7]. The survival rate α can be interpreted as the concentration of living cells at a certain time compared to its initial concentration. Traditionally, α in (3) is set to 1, whereas we modulate the Pennes bioheat equation with α since the effect of blood perfusion decreases when the tissue is thermally damaged.

Note that both the electrical conductivity σ and the thermal conductivity k are temperature-dependent. The electrical conductivity can be expressed as [5]:

$$\sigma\left(T\right)=\sigma_0\cdot\left[1+\sigma_1\left(T-T_0\right)\right] \tag{5}$$

The values of σ_0 and σ_1 are included in table II. Because of (5), the output of the thermal subproblem, i.e. the temperature T, influences the electrical conductivity which acts as an input of the electrical subproblem. The thermal conductivity is modeled as follows [5]:

$$k\left(T\right)=k_0+k_1\left(T-T_0\right) \tag{6}$$

The values of k_0 and k_1 are both included in table II as well. Since k is a part of the first term of (3), this leads to an entanglement of the input and output of the thermal subproblem. On the other hand, the output of the electrical subproblem, i.e. the electrical potential ϕ, causes Joule heating q_E acting as an additional heat source in the thermal subproblem: again coupling arises. Fig. 2 illustrates how the different parts of the model are entangled to each other resulting in a complex overall numerical model.

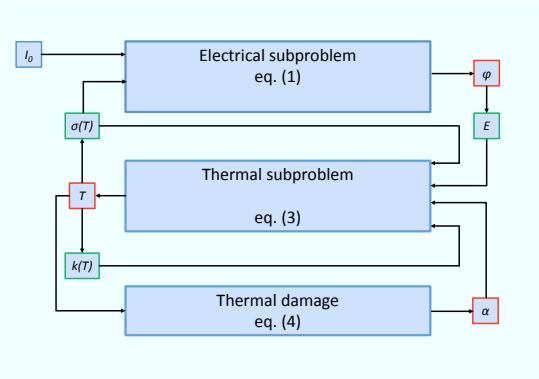

Fig. 2. Schematic overview of the entanglements of the numerical model of RFA.

B. Numerical methods

Equations (1) and (3) are solved numerically by the finite difference method. A central approximation of the derivatives is performed on a regular cubic grid. The finite difference grid can originate from magnetic resonance images where we associate a certain material property to each voxel. This can be processed using common software packages e.g. SPM8 [8]. However, we can also work with computer-generated geometries to test our numerical methods.

The differential operators of the Poisson equation (1) are approximated by finite difference operators, e.g.:

$$\left.\frac{\partial^2 V}{\partial x^2}\right|_i\approx\frac{1}{h_x^2}\left(V\left(x_{i+1}\right)-2V\left(x_i\right)+V\left(x_{i-1}\right)\right) \tag{7}$$

which is a central approximation on a regular cubic grid with spacing h_x. By means of analogous approximations, the left-hand side of (1) in a certain grid point can be expressed by the electrical conductivities and the potentials in the grid point and its six nearest neighbors [9]. Following the approach of [9], the original Poisson equation is thus transformed in a system of linear equations:

$$\left[A\right]\cdot\left[\Phi\right]=\left[B\right] \tag{8}$$

where A only depends on the electrical conductivities and the grid spacing, Φ contains the unknown electrical potentials and B contains the two current sources of bipolar RFA. Due to the sparsity corresponding with the finite difference approach, we are able to solve this system by means of the Preconditioned Biconjugate Gradient Stabilized Method (Preconditioned BiCGSTAB) [10]. This has proven to be a computationally efficient and stable method [10].

The thermal model (3) consists of a time-dependent partial differential equation of the following type:

$$\frac{\mathrm{d}T}{\mathrm{d}t}=f\left(t\right) \tag{9}$$

To solve this equation, we use the modified midpoint method. This method calculates the temperature at a certain moment in time $t+H$ based on the value at t:

$(t_{\text{start}} \rightarrow t_{\text{next}} = t_{\text{start}} + H)$. We divide this time period H in N equidistant substeps with time difference $\Delta t = \frac{H}{N}$:

$$[t_0 = t_{\text{start}} \quad t_1 \quad \dots \quad t_{\text{N}-1} \quad t_{\text{N}} = t_{\text{next}}] \tag{10}$$

The first step of the modified midpoint method is executed as follows:

$$T(t_1) = T(t_0) + \Delta t\, f(t_0) \tag{11}$$

The following steps have a different formulation:

$$T(t_n) = T(t_{n-2}) + 2\Delta t\, f(t_{n-1}) \quad \forall n \in \{2, \dots, N\} \tag{12}$$

At the end of each time step a Gragg-smoothing is performed to damp the oscillating errors [11]:

$$T(t_N) = \frac{1}{2}\left[T(t_N) + T(t_{N-1}) + \Delta t\, f(t_N)\right] \tag{13}$$

Note that for the calculation of (3), the function f of (9) still contains spatial derivatives. Similar to the numerical method of the electrical model, we use the central approximation of the derivatives on the same regular cubic grid.

III. PULSED CURRENTS

So to increase the efficacy, i.e. the control of size and shape of the ablation zone, we propose the concept of pulsed currents. The current is switched on until the maximum temperature in the liver reaches 80 °C. Next, the current is switched off during a fixed period, the switch-off time τ_f. The amplitude of the applied current profile is graphically represented in Fig. 3.

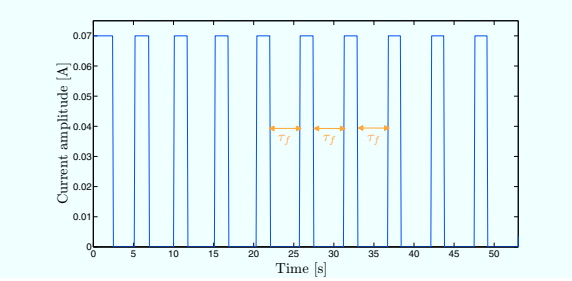

Fig. 3. Amplitude of pulsed currents with a fixed switch-off time τ_f.

The longer the switch-off time τ_f, the wider the temperature distribution in space and thus the larger the ablation region. However, the absolute temperature will decrease as well resulting in less thermal damage. Consequently, a trade-off is present. Our numerical methods allow to calculate the influence of the different switch-off times on the thermal damage for fixed needle positions.

IV. RESULTS AND DISCUSSION

Using the developed numerical methods we are able to perform numerical experiments on tessellated geometries of $101 \times 101 \times 101$ cubic voxels with a spatial discretization of 1 mm. A cross section of a computer-generated geometry is depicted in Fig. 4. Each color represents a different tissue which is indicated on the figure.

To assess the influence of pulsed currents, we will first study bipolar RFA in the absence of these pulsed currents.

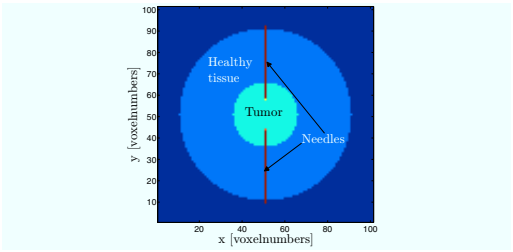

Fig. 4. Cross section of a computer-generated geometry.

The numerical methods allow to investigate the effect of the distinct material parameters. Fig. 5 illustrates the effect of the temperature-dependent electrical conductivity σ of (5). Here, the temperature variation of one voxel in time is depicted in two seperate cases: a temperature-independent σ ($\sigma_1 = 0\,\text{K}^{-1}$) and a temperature-dependent σ ($\sigma_1 = 0.015\,\text{K}^{-1}$). The ascending limb of the two curves is due to the q_E heat

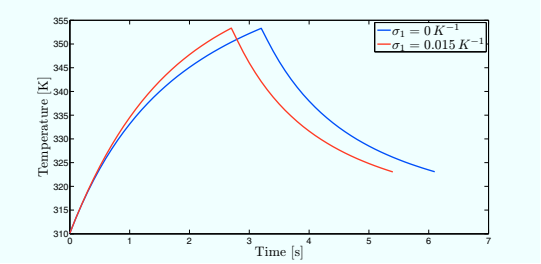

Fig. 5. Comparison of the temporal temperature profile between a geometry with a temperature-independent σ and a temperature-dependent σ.

source of (3), whereas the descending limb takes places when no current is applied. In the latter case the dominating effects are described by the first two terms of (3). Fig. 5 clearly illustrates the importance and the non-negligible effect of the temperature-dependent σ.

Another material property is studied in Fig. 6. This figure shows the temperature profile at a fixed moment in time along the line that connects the two needles in the cross section of Fig. 4. We observe that the bipolar RFA technique is very local, i.e. the temperature rise due to the injection of currents is constrained to a small region of the order of millimeters. This figure also illustrates the influence of inhomogeneity (healthy tissue with tumor versus completely healthy tissue) of material parameters on the temperature distribution.

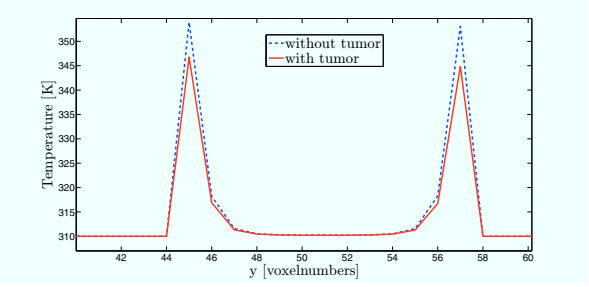

Fig. 6. Comparison of a temperature profile in the case of a geometry with a tumor and without a tumor.

To overcome the local behavior and to have more control over the size and shape of the ablation zone, we apply pulsed currents with different fixed switch-off times. Large differences are present between the various switch-off times as depicted in Fig. 7. Here the survival rate α is numerically determined in the center of the geometry at equal distance of both needle tips which is the best point to assess the locality of the therapy modality. Clearly, there is an optimal switch-off time (in this case $\tau_f = 0.5\,\mathrm{s}$) which reduces the survival rate of the tumoral tissue compared to the other switch-off times. Optimizing this switch-off time thus contributes to a more efficient treatment.

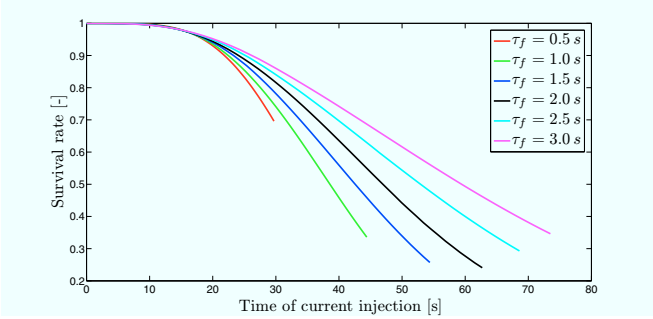

Fig. 7. Survival rate as function of the current injection time in the center of the simulation environment.

Fig. 8 illustrates the thermal damage in the central cross section of a smaller geometry ($51 \times 51 \times 51$ voxels) at different number of pulses with the optimized switch-off time. In the beginning, the ablation zones are restricted to the regions close to the needle. Due to the influence of an optimized switch-off time, a temperature build-up arises in the intermediate non-ablated zone: the ablation zones can overlap with each other. This overlap increases when the number of pulses increases. After 50 pulses the individual ablation zones disappear. This eventually results in one large cylindrical ablation zone when the amount of pulses is augmented. Our concept could help to treat larger tumors with an increased efficacy and thus has the potential to be incorporated in clinical practice as a computer-supported bipolar RFA treatment.

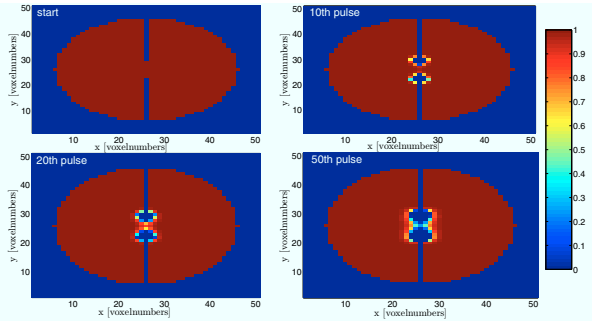

Fig. 8. Spatial distribution of the survival rate in the central cross section.

V. CONCLUSIONS

This work presents numerical methods for the interpretation of bipolar RFA. The numerical model consists of two subproblems describing the electrical and thermal phenomena. Both problems are simultaneously solved by means of a finite difference method. Based on the numerical results, bipolar RFA gives rise to a very local ablation region. Improvement of bipolar RFA is provided by using pulsed currents with fixed switch-off times. Due to the large differences between different switch-off times, an optimal switch-off time can be identified for each patient geometry, material parameters and needle positions. Numerical results confirm that the current profile with the optimal switch-off time leads to a larger ablation zone. Consequently, the computer-supported bipolar RFA increases the efficacy of the treatment of liver cancer.

In the future, we will perform ex-vivo experiments to confirm our concept of pulsed currents. Furthermore, particular attention will be paid to study this concept in a needle configuration that is applicable in clinical practice.

ACKNOWLEDGMENT

Frederik Soetaert is a Ph.D. fellow of the Research Foundation - Flanders (FWO). Guillaume Crevecoeur is a postdoctoral researcher of the Research Foundation - Flanders (FWO).

REFERENCES

[1] J. Ferlay, H. Shin, F. Bray, D. Forman, C. Mathers, and D. Parkin. GLOBOCAN 2008 v2.0, Cancer Incidence and Mortality Worldwide: IARC CancerBase No. 10. Lyon, France: International Agency for Research on Cancer; 2010.

[2] H. B. El-Serag, "Hepatocellular carcinoma," *New England Journal of Medicine*, vol. 365, no. 12, pp. 1118 – 1127, 2011.

[3] A. P. O'Rourke, D. Haemmerich, P. Prakash, M. C. Converse, D. M. Mahvi, and J. G. Webster, "Current status of liver tumor ablation devices," *Expert Review of Medical Devices*, vol. 4, no. 4, pp. 523 – 537, 2007.

[4] H. H. Pennes, "Analysis of tissue and arterial blood temperatures in the resting human forearm," *Journal of Applied Physiology*, vol. 1, no. 2, pp. 93 – 122, 1948.

[5] D. Haemmerich and B. J. Wood, "Hepatic radiofrequency ablation at low frequencies preferentially heats tumour tissue," *International Journal of Hyperthermia*, vol. 22, no. 7, pp. 563 – 574, 2006.

[6] S. Tungjitkusolmun, S. T. Staelin, D. Haemmerich, J. Z. Tsai, J. G. Webster, F. T. Lee, D. M. Mahvi, and V. R. Vorperian, "Three-Dimensional finite-element analyses for radio-frequency hepatic tumor ablation." *IEEE Transactions on Biomedical Engineering*, vol. 49, no. 1, pp. 3 – 9, 2002.

[7] I. dos Santos, D. Haemmerich, D. Schutt, A. F. da Rocha, and L. R. Menezes, "Probabilistic finite element analysis of radiofrequency liver ablation using the unscented transform," *Physics in Medicine and Biology*, vol. 54, no. 3, pp. 627 – 639, 2009.

[8] K. Friston, J. Ashburner, S. Kiebel, T. Nichols, and W. Penny, Eds., *Statistical Parametric Mapping: The Analysis of Functional Brain Images*. Academic Press, 2007.

[9] H. Saleheen and K. Ng, "A new three-dimensional finite-difference bidomain formulation for inhomogeneous anisotropic cardiac tissues," *IEEE Transactions on Biomedical Engineering*, vol. 45, no. 1, pp. 15 – 25, 1998.

[10] N. De Geeter, G. Crevecoeur, and L. Dupré, "An efficient 3-D eddy-current solver using an independent impedance method for transcranial magnetic stimulation," *IEEE Transactions on Biomedical Engineering*, vol. 58, no. 2, pp. 310 – 320, 2011.

[11] G. Dahlquist and Å. Björck, *Numerical Methods*. Prentice–Hall, Inc., 1974.